

Multifractality of correlated two-particle bound states in quasiperiodic chains

Diana Thongjaomayum,¹ Sergej Flach,^{1,2} and Alexei Andreanov^{1,2}

¹Center for Theoretical Physics of Complex Systems, Institute for Basic Science (IBS), Daejeon, Korea, 34126

²Basic Science Program, Korea University of Science and Technology (UST), Daejeon, Korea, 34113

(Dated: May 27, 2022)

We consider the quasiperiodic Aubry-André chain in the insulating regime with localised single-particle states. Adding local interaction leads to the emergence of extended correlated two-particle bound states. We analyse the nature of these states including their multifractality properties. We use a projected Green function method to compute numerically participation numbers of eigenstates and analyse their dependence on the energy and the system size. We then perform a scaling analysis. We observe multifractality of correlated extended two-particle bound states, which we confirm independently through exact diagonalisation.

I. INTRODUCTION

Understanding the transport properties of quantum disordered or inhomogeneous systems has been an active topic of research since the discovery of Anderson localisation (AL). AL describes the arrest of transport in a single particle system due to disorder or inhomogeneous potential which renders all the eigenstates in one and two space dimensions exponentially localised.¹ The original work of Anderson triggered a sequence of theoretical studies and by now the single particle case is well understood.² The important and much harder question is the stability of modification of AL in the presence of many-body interactions. Decades of research culminated in the opening of the field of Many Body Localisation.³⁻⁵ Interestingly one of the strongly debated issues is the possible existence of 'bad' metallic states which are non-ergodic or simply multi-fractal.^{3,5}

A notorious issue with MBL related studies is the computational complexity due to the exponential proliferation of the Hilbert space dimension with increasing numbers of particles and system size. A legitimate and complementary approach is therefore to consider only few interacting particles, which allows to increase the system size beyond the limits set by typical MBL models. Three main directions with single particle localisation in one dimension have been explored: genuine AL due to uncorrelated disorder,² Wannier-Stark (WSL) localisation due to an external dc field,⁶ and Aubry-André (AAL) localisation due to a quasiperiodic external potential.⁷ Genuine AL yields a nontrivial increase of the localisation length for two interacting particles with still unsettled scaling details.⁸⁻¹¹ Two interacting particles yield no localisation change for WSL with interaction, only affecting the Bloch oscillation periods.¹² At variance, AAL with quasiperiodic potentials showed an unexpected transition from localisation (zero interaction) to delocalisation (non-zero interaction).¹³ These findings were later confirmed in Ref. 14 which provided additional indications for the fractal nature of the delocalised eigenstates.

Are these the seeds of a bad metal and the MBL transition from above? A hint might be obtained from the striking similarity of the phase diagram of correlated

metallic two-particle bound states in Fig. 4 of Ref. 13 and the phase diagram of an MBL phase which was experimentally assessed for interacting fermions in optical quasiperiodic potentials in Fig. 4 of Schreiber *et al* in Ref. 15. In the present study we attempt to add more conclusive arguments which aim at a positive answer for the above question for quasiperiodic potentials. We confirm the fractal character of the two-particle spectrum and the fractality of some of the two-particle states. We rely on the projected Green function method,¹⁶ originally developed to analyse the localisation length of two interacting particles in the AL case. The paper is organised as follows: we introduce the tools and other necessary means in Sec. II. Section III benchmarks these tools in the single particle case against the exact results and exact diagonalisation. In Sec. IV we analyse the two interacting particles case. This is followed by conclusions.

II. SETTING THE STAGE

The starting point is a single particle placed in a quasiperiodic potential with the Aubry-André Hamiltonian⁷

$$\mathcal{H}_0 = \sum_n (|n\rangle\langle n+1 + \text{h.c.}) + \sum_m h_m, \quad (1)$$
$$h_n = \lambda \cos(2\pi\alpha n + \beta),$$

where λ is the strength of the potential, α is an irrational number ensuring quasiperiodicity of the potential. We choose $\alpha = (\sqrt{5}-1)/2$, the golden ratio and we fix the hopping strength $t = 1$. Depending on the strength of the potential λ the eigenstates are all delocalised ($\lambda < 2$) or localised ($\lambda > 2$) with localisation length $\xi_1 = 1/\ln(\lambda/2)$, which is the same for all the eigenstates.⁷ Finally β is a phase which can be varied to generate different realisations of the quasiperiodic potential. In numerical studies with finite system size the choice of β will affect localised and sparse, fractal or multi-fractal extended states. In the present study involving critical states we use averaging over different values of β , that we denote as $\overline{\dots}$, to improve statistics.

We now add the interactions and consider two interacting bosons. We choose the onsite Hubbard interaction of strength u . The total Hamiltonian is given by

$$\begin{aligned} \mathcal{H} &= \mathcal{H}_0 \otimes \mathcal{H}_0 + uP \\ &= \sum_{n,m} (|n, m\rangle\langle n+1, m| + |n, m\rangle\langle n, m+1| + \text{h.c.}) \\ &\quad + \sum_{n,m} |n, m\rangle (h_n + h_m) \langle n, m| + uP, \end{aligned} \quad (2)$$

where $|n, m\rangle$ is a basis state with two particles at site n, m , and h_n is the onsite Aubry-André potential at site n given by Eq. (1). P is the projection operator defined as $P|n, m\rangle = \delta_{nm}|n, m\rangle$ that enforces the onsite Hubbard interaction.

The authors of the work Ref. 13 used exact diagonalisation and unitary evolution of wavepackets to study the two-particle properties of the model (2). The exact diagonalisation limited the largest system sizes achievable to $N \approx 250$, imposed by the efficiency of full diagonalisation of the Hamiltonian matrix (2). Later Frahm in Ref. 14 implemented a dedicated sparse diagonalisation algorithm based on Green functions^{16,17} to handle large sizes, up to $N = 10946$, of the Hamiltonian (2). We follow the original approach of Ref. 16. We extract the relevant two-particles properties from the projected two-particle Green function, which is obtained as a projection of the full Green function $G = (E - \mathcal{H})^{-1}$ onto doubly occupied states (relying crucially on the fact that the Hubbard interaction is proportional to the projector P):

$$\tilde{G} = \frac{\tilde{G}_0}{1 - u\tilde{G}_0}. \quad (3)$$

Here $\tilde{G} = PGP$ and $\tilde{G}_0 = PG_0P$; G_0 is the non-interacting two particle GF which can be obtained by straightforward diagonalisation of the single particle Hamiltonian (1). Knowing the single particle eigenenergies $\{E_\mu\}$ and eigenfunctions $\{\phi_\mu(n)\}$ we compute G_0 as follows:

$$\begin{aligned} \langle n, n|G_0(E)|m, m\rangle &= \sum_{\mu, \nu} \frac{\phi_\mu(n)\phi_\nu(n)\phi_\mu^*(m)\phi_\nu^*(m)}{E - E_\mu - E_\nu} \\ &= \sum_{\mu} \phi_\mu(n)g_0(E - E_\mu)\phi_\mu(m), \quad (4) \\ g_0(E) &= \frac{1}{E - \mathcal{H}_0} = \sum_{\nu} \frac{\phi_\nu^*(n)\phi_\nu(m)}{E - E_\nu}. \end{aligned}$$

The reordering of the terms in the second line is done to reduce the complexity of the computation from the original $O(N^4)$ to $O(N^3)$,⁹ since the single particle Green function g_0 can be efficiently evaluated using tridiagonal matrix inversion of the single particle Hamiltonian (1). This approach allows us achieve system sizes as large as $N = 7000$.

In the insulating regime the exponential decay of the projected Green's function \tilde{G} was used to extract the

two interacting particles (TIP) localisation length.^{11,16,18} Here we are aiming to investigate TIP eigenstates which we expect to be extended in a predominantly insulating region,¹³ therefore \tilde{G} might not decay or the decay might not be exponential. Consequently we adopt a different measure:¹¹ Interpreting the projected Green function \tilde{G} as a probability density function we define the participation number $I_{q=2}$ and its higher moments $I_{q>2}$ as

$$I_q = \left(\sum_k |\tilde{g}(k)| \right)^q / \sum_k |\tilde{g}(k)|^q, \quad (5)$$

where $\tilde{g}(k) = \langle n, n|\tilde{G}|n+k, n+k\rangle$. We shall use I_2 and higher moments that are always well defined to analyse the TIP states. To distinguish I_q from the conventional participation number we will refer to it as the Green function participation number (GPN). However before we can proceed to the two particle case, we need to confirm that I_2 is a valid measure of localisation of an eigenstate Ψ , similar to the conventional participation number:

$$\text{PN}_q = \sum_{nm} |\Psi_{nm}|^{2q}, \quad (6)$$

e.g. that I_2 can distinguish between extended, (multi)fractal and localised states.

III. SINGLE PARTICLE: BENCHMARKING

To confirm that the above defined participation number I_q is a valid probe of localisation properties of eigenstates we first consider the single particle case. To achieve this we benchmark two single-particle quantities: localisation length – analytical and numerical

$$\xi_1 = \frac{1}{\ln\left(\frac{\lambda}{2}\right)} \quad (7)$$

$$\frac{1}{\xi_1} = - \lim_{|n-m| \rightarrow \infty} \frac{\ln|\langle n|g_0|m\rangle|}{|n-m|}, \quad (8)$$

and participation number I_2 , which is defined similarly to its two particle version Eq. (5):

$$I_q = \left(\sum_k |g(k)| \right)^q / \sum_k |g(k)|^q, \quad (9)$$

where $g(k) = \langle n|g_0|n+k\rangle$. Our aim is to confirm that I_2 is a valid substitute for ξ_1 for localised states and it behaves like the conventional participation number for localised and extended states.

To prove that we consider 3 different values of the potential strength $\lambda = 1, 2, 2.5$, which correspond to delocalised, critical and localised regimes. For each λ we compute single particle eigenstates ψ and the Green function g_0 for energies $E \in [-3, 3]$ in steps of $\Delta E = 0.05$, scanning the entire single particle spectrum. This step size of 0.05 is chosen to be slightly bigger than the level spacing $\delta(N = 250) = 0.004$ and $\delta(N = 500) = 0.002$ for

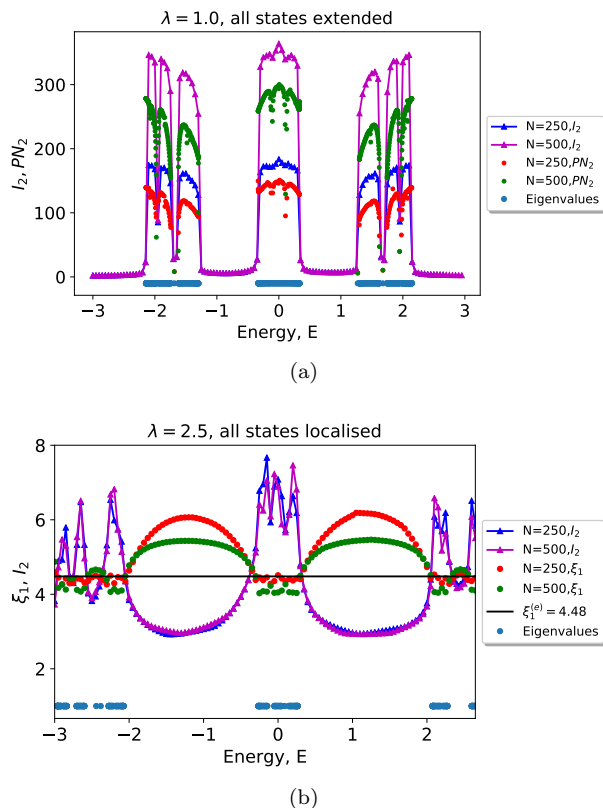


FIG. 1. (Colour online) Benchmarking of a single particle in the AA model: (a) $\lambda = 1$: I_2 and PN_2 for $N = 250, 500$. (b) $\lambda = 2.5$: Localisation length ξ_1 and I_2 for $N = 250, 500$. The black line represents the analytical value $\xi_1 = 4.48$. The participation number PN_2 behaves similarly to I_2 (not shown). The bottom blue/circular points in both (a) and (b) represent the spectrum of \mathcal{H}_0 for $N = 500$ and show the locations of the eigenstates.

the data presented in Fig. 1. From the Green function g_0 we evaluate ξ_1 and I_2 and from the eigenstates ψ we compute PN_2 . Figure 1(a) shows the results for $\lambda = 1$ for which all the single particle eigenstates are extended. The plot of Fig. 1(a) shows I_2 and PN_2 vs E for system sizes $N = 250, 500$. The bottom circular/blue points of Fig. 1(a) show the single-particle spectrum obtained from the full diagonalisation of \mathcal{H}_0 for $N = 500$. We see that both participation numbers PN_2 and I_2 drop to zero in the gaps of the spectrum of \mathcal{H}_0 , and increase with the system size for energies where eigenstates are present. We observe $I_2 > PN_2$ in general.¹¹ Figure 1(b) compares the same quantities for $\lambda = 2.5$ where the entire spectrum is localised. Fig. 1(b) shows I_2 and ξ_1 against E for $N = 250, 500$. The eigenenergies are plotted at the bottom of Fig. 1(b) (light blue points). The black line is the exact localisation length $\xi_1^{(e)} = 1/\ln(1.25) \approx 4.48$. The localisation length ξ_1 evaluated from the Green function (8) is close to the exact value $\xi_1^{(e)}$ for energies close to the eigenenergies of the system, while I_2 is systematically larger than ξ_1 , but is roughly of the same order,

and does not scale with the system size N . In the gaps of the exact spectrum, I_2 drops to zero which is expected since there are no eigenstates corresponding to these energies and contributions from the eigenstates are negligible. However ξ_1 , defined by Eq. (8), gives completely wrong value in the gaps of the single particle spectrum as seen in Fig. 1(b). This is clearly an artefact of the exponential fitting of g_0 that does not decay exponentially inside the gaps of the spectrum of \mathcal{H}_0 . The behaviour of the participation number PN_2 is very similar to I_2 (not shown). For the critical case $\lambda = 2$, the behaviour of ξ_1 and I_2 is similar to that of the delocalised $\lambda = 1$ case.

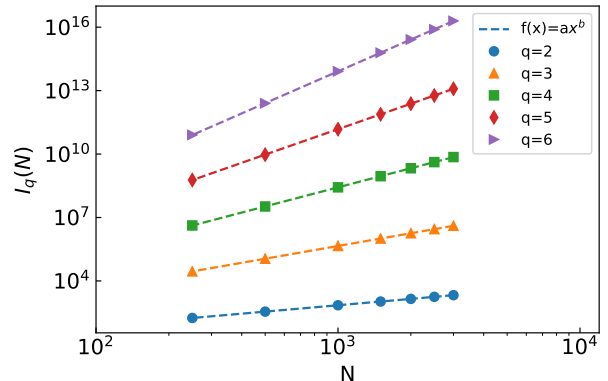


FIG. 2. (Colour online) Participation number $I_q(N)$ (symbols) vs system size $N = 250$ to 3000 for $q = 2, 3, 4, 5, 6$ and the power law fits $I_q(N) = aN^b$ (dashed lines) for $\lambda = 1$. The power-law fit works well also for $\lambda = 2, 2.5$ (not shown).

This rough comparison lends support to the validity of I_2 as a substitute for the participation number PN_2 . To strengthen this support we look into the scaling of the participation numbers PN_q with the power q , which also distinguishes extended, localised and (multi)fractal states: $PN_q = aN^{\mathcal{D}_q(q-1)}$ where \mathcal{D}_q is the fractal dimension of the state, and $\mathcal{D}_q = 0$ corresponds to localised state, $\mathcal{D}_q = 1$ corresponds to delocalised states, $0 < \mathcal{D}_q < 1$ - to (multi)fractal states. We verify whether a similar scaling holds for I_q and try the fit $I_q = aN^{\mathcal{D}_q(q-1)}$ for all the three regimes: $\lambda = 1, 2, 2.5$. We pick the energy E_{\max} corresponding to the maximum of I_2 for the largest system size considered, $N = 3000$, since we want to probe the most delocalised states in an otherwise localised regime (this choice is only relevant for $\lambda = 2.5$ where all eigenstates are localised), and use this value E_{\max} to evaluate \mathcal{D}_q for smaller system sizes. For every λ we compute I_q for $q = 2, 3, 4, 5, 6$ and for a range of system sizes $N = 250$ to 3000 . The results are shown in Fig. 2: we see a clear power law scaling of I_q with N for every individual value of q . Next we fit these data for several system sizes to extract \mathcal{D}_q for the values of $\lambda = 1, 2, 2.5$. Similarly we evaluate the \mathcal{D}_q from the scaling of PN_q with system size. The PN_q are computed from exact diagonalisation of a single particle Hamiltonian (1). The results are summarised in Fig. 3: both

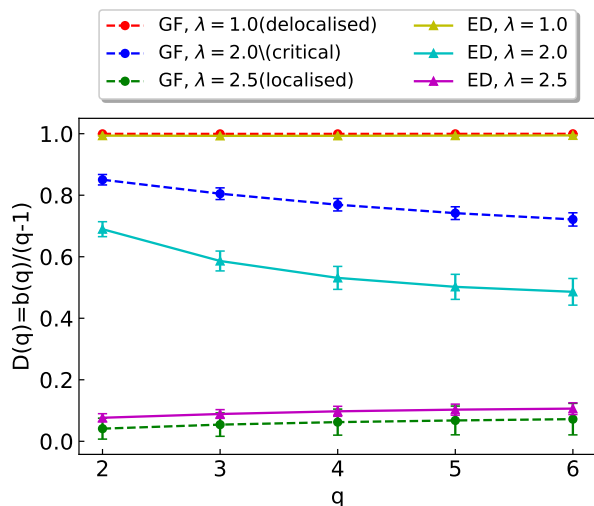


FIG. 3. (Colour online) Fractal dimension D_q vs q obtained from Green's function (GF) and exact diagonalisation (ED) in extended (red/yellow), critical (blue/cyan) and localised (green/magenta) regimes for the single particle case. The dimension D_q is q -independent and equal to zero(one) in the extended(localised) regime and has a non-trivial dependence on q at the criticality, $\lambda = 2$. This is a similar behaviour to the dimension \mathcal{D}_q computed from the PN_q .

methods agree - $\mathcal{D}_q \approx D_q \approx 1$ for $\lambda = 1.0$ - as it should be for extended states, $\mathcal{D}_q \approx D_q \approx 0.0$ - for the localised case $\lambda = 2.5$, and q -dependent \mathcal{D}_q , D_q for the critical value $\lambda = 2.0$ where multifractality is expected.

These results indicate that I_2 can be used as a substitute for the localisation length ξ_1 and the participation number PN_q in the single particle case. We assume that this is also the case for two interacting particles and verify this assumption self-consistently. Therefore in what follows we will study the behaviour of I_2 and higher moments $I_{q>2}$.

IV. TWO INTERACTING PARTICLES: SELF-SIMILARITY OF THE SPECTRUM AND FRACTALITY OF THE EIGENSTATES

We now turn to the case of two particles with the on-site Hubbard interaction. Earlier work¹³ has reported the emergence of metallic states in the single-particle insulating regime ($\lambda > 2$). This conclusion was based on exact diagonalisation of systems up to $N = 250$ (up to $N = 1000$ with sparse diagonalisation) sites and analysis of the spreading of time-evolved wave packets scanned in the entire range of interactions $0 < u < 12$ for several values of potential strength $\lambda \in [1.8, 3]$. These results were enhanced by Frahm¹⁴, who performed diagonalisation of systems up to $N = 10946$ sites and confirmed the presence of delocalised states.

We start our analysis with a cross check of Ref. 13 and evaluate the participation number I_2 from \tilde{G}_{nm} (5) for

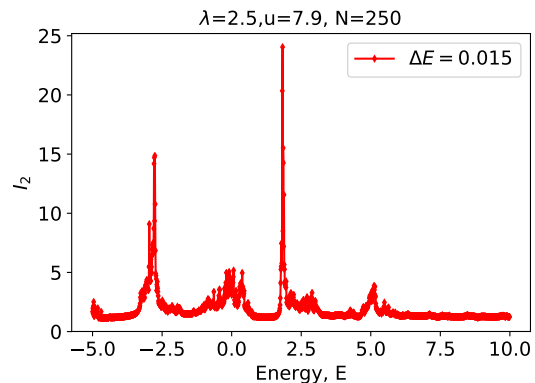


FIG. 4. (Colour online) Participation number I_2 vs energy E for two interacting particles. The peaks signal the emergence of delocalised states in the otherwise localised spectrum.

$\lambda = 2.5$, $u = 7.9$ and 1000 values of energy $E \in [-5, 10]$. The results are averaged over 10 disorder realisations, e.g. values of β , see Eq. (1). In Fig. 4 we see a minibands structure with the few energies where the value of I_2 is relatively large, similarly to the findings of Ref. 13 thereby lending further support to the use of I_2 as a probe of the extent of the eigenstates. We identified two values of energy, $E_1 \approx 1.8$, $E_2 \approx -2.8$ where I_2 achieves its local maximum (Fig. 4), suggesting the emergence of delocalised states at these energies.

To get a better insight into the nature of these emerging states we study the fine structure in the vicinity of the I_2 peaks. To extract this fine structure we start with a small system size and identify the peaks of I_2 by discretising the energy range. Next we zoom into the energy range around one of the peaks by using a finer energy discretisation. This procedure is repeated several times for increasing system sizes N . Such analysis of fine details of the structure of I_2 is possible thanks to the usage of the projected Green functions. To be specific for the peak of I_2 at $E_1 \approx 1.8$, we started with a range of energies $[1.821 : 1.8225]$ for the smallest system size $N = 250$. We observe the emergence of new peaks which become prominent as the size is increased to $N = 500$ and $N = 1000$ (Fig. 5(a)). Zooming in the energy range around one peak ($E \in [1.8212, 1.8215]$, marked by black rectangular box on Fig. 5) the original peak resolves into several peaks for larger system size $N = 3000$, Fig. 5(b). Repeating this procedure two more times for the peaks marked by the black boxes, we obtain Fig. 5(c-d) for $N_{\text{max}} = 7000$. The largest I_2 is observed at $E_1 = 1.8214063$ for $N = 7000$. Upon every iteration we observe the emergence of finer structure in I_2 as we are zooming in energy. This strongly suggests the fractal nature of participation number I_2 as a function of energy E and consequently the spectrum of the delocalised states at these energies.

In the original work, Ref. 13, these states were assumed delocalised based on the analysis of wave packet spreading. Subsequent work in Ref. 14 performed a more de-

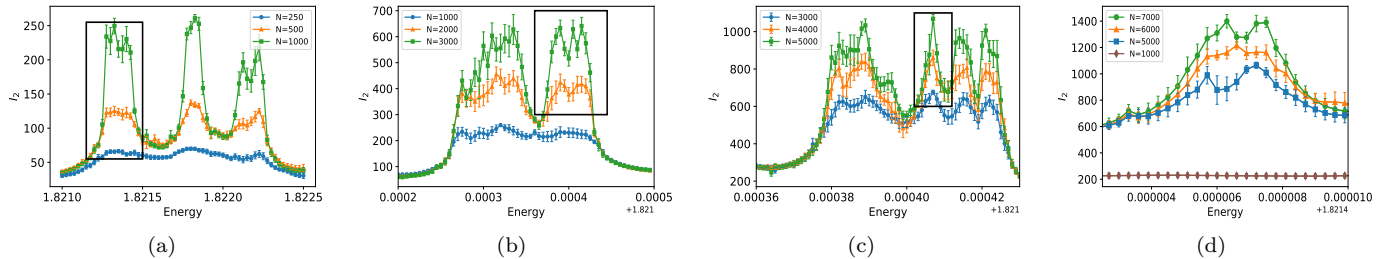


FIG. 5. (Colour online) Average Green's function participation number I_2 around energy $E_1 \approx 1.8$ at $u = 7.9$. The energy range is zoomed in from left to right, with the maximum system size increasing from $N = 1000$ (left) to $N = 7000$ (right) and the resolution in energy reaching $\Delta E = 3 \times 10^{-7}$ for the rightmost plot. The errorbars correspond to the disorder average. The peaks of I_2 resolve into fine structure with subpeaks upon every iteration of zooming in.

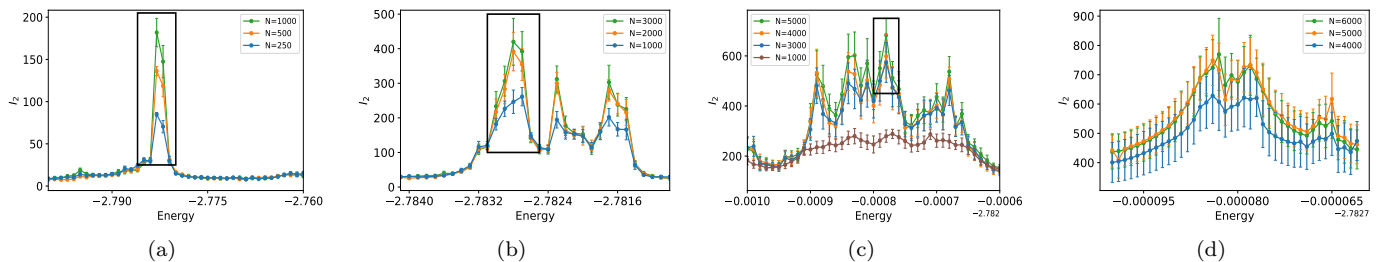


FIG. 6. (Colour online) Average Green's function participation number I_2 around energy $E_2 \approx -2.8$ at $u = 7.9$. The energy range is zoomed in from left to right, with the maximum system size increasing from $N = 1000$ (left) to $N = 6000$ (right) and the resolution in energy reaching $\Delta E = 10^{-6}$ for the rightmost plot. The errorbars correspond to the disorder average. The peaks of I_2 resolve into fine structure with subpeaks upon every iteration of zooming in.

tailed analysis and confirmed this conclusion and also provided some indications of fractality of these states based on the fitting i) inverse participation ratio in position representation denoted as ξ_x , ii) inverse participation ratio in energy representations, ξ_E (for details see Ref. 14). To clarify the fractal nature of these states we consider the largest I_2 at energy $E = E_1$ and compute $I_q(N)$ for $q = 2, 3, 4, 5, 6$ and several system sizes N at this energy. Assuming the multifractal ansatz for the participation number $I_q(N) \sim aN^{D_q(q-1)}$ we extract the fractal dimension D_q from numerical values $I_q(N)$, similarly to how it was done in the single particle case, see Fig. 2. The extracted values of D_q are shown as red points (circles) in Fig. 7 with the error bars of the fit. We observe that $D_q < 1$ and q -dependent suggesting that the corresponding eigenstates at this energy are multifractal. In Ref. 14 a power-law fit of ξ_x and ξ_E with system size N with $N_{\max} \approx 10000$ was computed. The extracted values of the power-law exponents $a_{x,E} < 1$ for energies $E = -2.787, 1.817$ and interaction $u = 7.9$ suggested that these states were fractal.

In the same way, energies around $E_2 \approx -2.8$ were analysed, up to system size $N_{\max} = 6000$. The results were averaged over 10 disorder samples, e.g. values of β (see Eq. (1)). The results are shown in Fig. 6. We observe larger fluctuations in participation number I_2 as compared to $E_1 \approx 1.8$ which are shown with the error bars.

Also the dependence of I_2 on system size N is less prominent as compared to the global maximum of I_2 located at $E_1 \approx 1.8$ when the energy is zoomed in, even for the largest system size considered (Fig. 6c-d). The fractal dimension D_q extracted from I_q shows an almost flat dependence on q (green circles in Fig. 7), suggesting only fractal but not multifractal character of the state at this energy.

The Green function participation number results are indirect, since they do not probe the eigenstates directly. Their advantage is the much lower computational cost for larger system sizes as compared to the exact diagonalisation. Therefore to check our predictions on the fractality of the eigenstates independently we performed sparse diagonalisation around energies $E_1 = 1.8214063$ and $E_2 = -2.782783$, corresponding to the local maxima of I_2 for $N_{\max} = 7000$ and $N_{\max} = 6000$ respectively. Among the eigenstates extracted around these two energies, we systematically picked the ones with the largest PN_2 for all system sizes N since we aimed at the most delocalised eigenstates embedded into the predominantly localised ones. The power law fits of the participation number moments, $PN_q(N) \propto N^{D_q(q-1)}$ were calculated. The resulting values of D_q are shown in Fig. 7 as blue ($E = 1.8$) and green ($E = -2.8$) solid lines with triangular points. The dashed lines with points show D_q evaluated from the Green function participation numbers, red

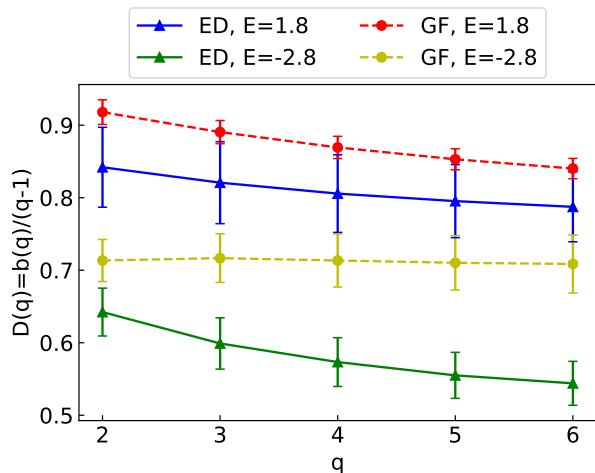


FIG. 7. (Colour online) Fractal dimensions D_q (extracted from the Green function participation number I_q) and \mathcal{D}_q (extracted from the participation number PN_q) vs q at energies $E_1 \approx 1.8$ and $E_2 \approx -2.8$. For E_1 both methods predict multifractality, while for E_2 the projected Green function method underestimates the fractality of the eigenstate.

for $E_1 = 1.8$ and yellow for $E_2 = -2.8$. We see that although the values of D_q and \mathcal{D}_q do not always agree perfectly, nevertheless D_q and \mathcal{D}_q imply at least fractality of the eigenstates that were previously considered delocalised.¹³ This also provides yet another evidence for the validity of I_q as a measure of localisation of eigenstates.

We elaborate further on the character of these fractal states appearing around $E_{1,2}$. Since the appearance of these states relies crucially on the interaction, we expect them to have a peculiar spatial pattern of the wavefunction amplitudes. Indeed we can construct many approximate localised eigenstates with two particles separated by one or more localisation lengths ξ_1 . Therefore the fractal states should have the two particles separated by at most the single particles localisation length ξ_1 . If we visualise the amplitudes of the two particles eigenfunction $|\Psi(x_1, x_2)|$ on a square lattice with coordinates x_1, x_2 , that correspond to the positions of the two particles, we expect the fractal states to be localised along the main diagonal $x_1 = x_2$, the fractal structure translating into some complicated pattern along the main diagonal. To verify this hypothesis we plotted two exact eigenstates with the largest PN_2 for $N = 3000$ in Fig. 8 ($u = 7.9$ and $E_1 \approx 1.8$ (top) and $E_2 \approx -2.78$). The axes denote the position of each of the two particles. We truncated amplitudes $|\Psi(x_1, x_2)| < 10^{-8}$ on the plots. These plots fully confirm our hypothesis outlined above, with most weight concentrated along the main diagonal, i.e. both particles being close to each other.

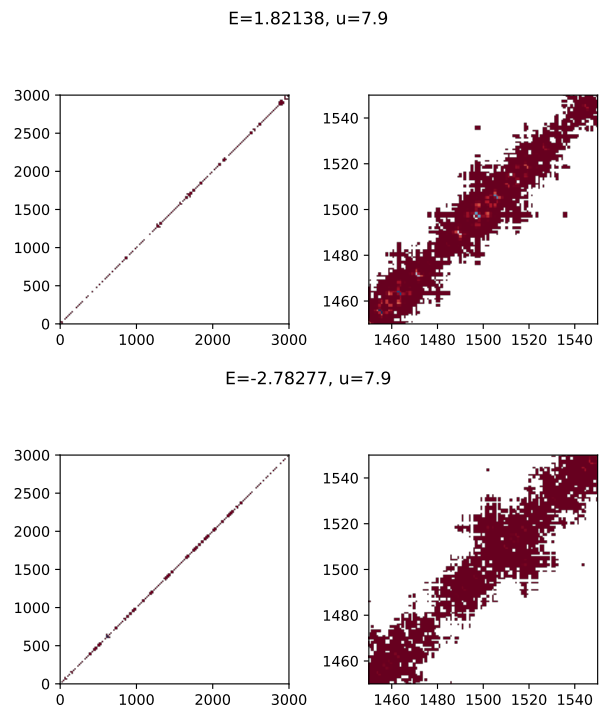


FIG. 8. (Colour online) The amplitudes $|\Psi(x_1, x_2)|$ of eigenstates computed for $N = 3000$ at $u = 7.9$ and corresponding to the local maxima of PN_2 . The X-axis and Y-axis denote the positions of the two particles - x_1 and x_2 - respectively. The larger amplitudes correspond to brighter colour. Values smaller than 10^{-8} were discarded. The energies are $E_1 \approx 1.8$ (top) and $E_2 = -2.78277$ (bottom). Left column: The eigenstate is localised along the main diagonal, e.g. the two particles stick together, but the pattern of the amplitudes along the diagonal is multifractal. Right column: the zoom into the left figure, highlighting the complex, multifractal pattern of the eigenfunction along the diagonal.

V. CONCLUSIONS

To conclude, we have shown that previously discovered metallic states of two interacting particles in an AA chain in the insulating single-particle region have a fractal structure. Furthermore unlike previous claims we find that these states are multifractal. This is verified by computing participation numbers from projected GF as well as from exact diagonalisation. An interesting open problem is the fate of these multifractal states at finite density where many-body localisation was reported at half-filling.¹⁹

As a side effect, we demonstrated that the projected Green functions can be used as a first probe to check the nature of eigenstates in an interacting Hamiltonian system having the advantage that larger system sizes can be targeted as compared to the computationally challenging exact diagonalisation.

ACKNOWLEDGMENTS

This work was supported by the Institute for Basic Science in Korea (IBS-R024-D1).

-
- ¹ P. W. Anderson, “Absence of diffusion in certain random lattices,” *Phys. Rev.* **109**, 1492–1505 (1958).
- ² B. Kramer and A. MacKinnon, “Localization: theory and experiment,” *Rep. Prog. Phys.* **56**, 1469–1564 (1993).
- ³ D.M. Basko, I.L. Aleiner, and B.L. Altshuler, “Metal-insulator transition in a weakly interacting many-electron system with localized single-particle states,” *Ann. Phys.* **321**, 1126 – 1205 (2006).
- ⁴ Dmitry A. Abanin, Ehud Altman, Immanuel Bloch, and Maksym Serbyn, “Colloquium: Many-body localization, thermalization, and entanglement,” *Rev. Mod. Phys.* **91**, 021001 (2019).
- ⁵ Fabien Alet and Nicolas Laflorencie, “Many-body localization: An introduction and selected topics,” *Comptes Rend. Phys.* **19**, 498 – 525 (2018).
- ⁶ Hidetoshi Fukuyama, Robert A. Bari, and Hans C. Fogedby, “Tightly bound electrons in a uniform electric field,” *Phys. Rev. B* **8**, 5579–5586 (1973).
- ⁷ Serge Aubry and Gilles André, “Analyticity breaking and anderson localization in incommensurate lattices,” *Ann. Israel Phys. Soc* **3**, 18 (1980).
- ⁸ D. L. Shepelyansky, “Coherent propagation of two interacting particles in a random potential,” *Phys. Rev. Lett.* **73**, 2607–2610 (1994).
- ⁹ K.M. Frahm, “Interaction induced delocalization of two particles: large system size calculations and dependence on interaction strength,” *Eur. Phys. J. B* **10**, 371–378 (1999).
- ¹⁰ D. O. Krimer, R. Khomeriki, and S. Flach, “Two interacting particles in a random potential,” *JETP Lett.* **94**, 406–412 (2011).
- ¹¹ Diana Thongjaomayum, Alexei Andreanov, Thomas Engl, and Sergej Flach, “Taming two interacting particles with disorder,” *Phys. Rev. B* **100**, 224203 (2019).
- ¹² Ramaz Khomeriki, Dmitry O. Krimer, Masudul Haque, and Sergej Flach, “Interaction-induced fractional bloch and tunneling oscillations,” *Phys. Rev. A* **81**, 065601 (2010).
- ¹³ Sergej Flach, Mikhail Ivanchenko, and Ramaz Khomeriki, “Correlated metallic two-particle bound states in quasiperiodic chains,” *EPL* **98**, 66002 (2012).
- ¹⁴ Klaus M. Frahm and Dima L. Shepelyansky, “Freed by interaction kinetic states in the harper model,” *Eur. Phys. J. B* **88**, 337 (2015).
- ¹⁵ Michael Schreiber, Sean S. Hodgman, Pranjal Bordia, Henrik P. Lüschen, Mark H. Fischer, Ronen Vosk, Ehud Altman, Ulrich Schneider, and Immanuel Bloch, “Observation of many-body localization of interacting fermions in a quasirandom optical lattice,” *Science* **349**, 842–845 (2015).
- ¹⁶ Felix von Oppen, Tilo Wettig, and Jochen Müller, “Interaction-induced delocalization of two particles in a random potential: Scaling properties,” *Phys. Rev. Lett.* **76**, 491–494 (1996).
- ¹⁷ W. E. Arnoldi, “The principle of minimized iteration in the solution of the matrix eigenvalue problem,” *Quart. Appl. Math.* **9**, 17–29 (1951).
- ¹⁸ Klaus M. Frahm, “Eigenfunction structure and scaling of two interacting particles in the one-dimensional anderson model,” *Eur. Phys. J. B* **89**, 115 (2016).
- ¹⁹ Shankar Iyer, Vadim Oganesyan, Gil Refael, and David A. Huse, “Many-body localization in a quasiperiodic system,” *Phys. Rev. B* **87**, 134202 (2013).